Absolute Measurement of Electron Cloud Density in a Positively-Charged Particle Beam

Michel Kireeff Covo[1,3], Arthur W. Molvik[1], Alex Friedman[1], Jean-Luc Vay[2], Peter A. Seidl[2], Grant Logan[2], David Baca[2], and Jasmina L. Vujic[3]

[1]*Lawrence Livermore National Laboratory, Heavy-Ion Fusion Virtual National, Laboratory, Livermore, California 94550, USA*

[2]*Ernest Orlando Lawrence Berkeley National Laboratory, Heavy-Ion Fusion Virtual National Laboratory, 1 Cyclotron Road, Berkeley, California 94720, USA*

[3]*University of California at Berkeley, 4155 Etcheverry Hall, MC 1730, Berkeley, California 94720, USA*

Clouds of stray electrons are ubiquitous in particle accelerators and frequently limit the performance of storage rings. Earlier measurements of electron energy distribution and flux to the walls provided only a relative electron cloud density. We have measured electron accumulation using ions expelled by the beam. The ion energy distribution maps the depressed beam potential and gives the dynamic cloud density. Clearing electrode current reveals the static background cloud density, allowing the first absolute measurement of the time-dependent electron cloud density during the beam pulse.

PACS numbers: 29.27.Bd, 29.30.Aj, 34.50.Dy, 41.75.Ak, 79.20.Rf

Beam halo and photons hitting the walls of accelerators or storage rings desorb gas and electrons. The desorbed and residual gas can be ionized. In some conditions the electrons can multiply and accumulate, deteriorating the beam quality, and coupling with

the beam to drive instabilities. Deleterious electron cloud effects (ECE) include electron-stimulated gas desorption, cloud-induced noise on instrumentation, tune shifts, instabilities and heat deposition on cryocooled components [1].

ECE were observed in the proton storage rings at BINP [2], the intersecting storage rings at CERN [3], the proton storage ring at LANL [4], the relativistic heavy ion collider at BNL [5], the photon factory at KEK [6,7], the low energy ring at KEKB [8], and other storage rings. They can potentially limit the performance of the spallation neutron source at ORNL [9,10], and the large hadron collider (LHC) at CERN [11], and have been subject of and featured in various meetings (EPAC 2004, ECLOUD'04, ICFA-HB2004, HHH2004, PAC05, DIPAC2005, etc).

Measurements of electron cloud density, in combination with simulation and theory, are fundamental for understanding ECE. Inferred densities from electron wall flux measurements and average velocity are only rough estimates [12]. Quantitative measurements of electron density have been made only between bunches by sweeping them towards a detector with a pulsed electrode [13] or by selecting high energy electrons when the bunch pattern emerges [14]. The measured electron cloud lifetime sometimes exceeds theoretical expectations, suggesting that low-energy electrons may have a long survival time because of their high reflectivity from walls [13,15].

We developed a new method, designated the "RFA technique", that provides the first absolute measurement of time-dependent electron cloud density accumulation during the beam pulse. The beam impact on gas produces cold ions from ionization and charge exchange that are expelled by the beam space-charge potential, converting potential energy to kinetic energy when they reach the walls in few hundred nanoseconds. As electrons accumulate, the beam potential decreases and so does the energy of the expelled ions [16]. The electron density as a function of time is obtained from the beam potential decay measurement accounting for the ion and electron transverse distributions. The dynamic density can be supplemented and corroborated by the static background density obtained from clearing electrodes measurements, giving the absolute electron density.

This technique is straightforward for possible superbunch operation of hadron colliders (LHC in construction at CERN and 12GeV Proton Synchrotron Experiment at KEK) and the High Current Experiment (HCX) [17] at LBNL, where the time to expel ions is shorter than the beam duration. It can also be applied to multibunched beams, where the bunch duration is shorter than the ion expulsion time, but this requires modeling ion expulsion energies.

Fig. 1 shows the magnetic transport section from HCX with background pressure of ~ 5×10^{-7} torr that is being used to identify and quantify sources of electrons, and validate three-dimensional self-consistent simulations of ECE inside quadrupole magnets, using the WARP code [18].

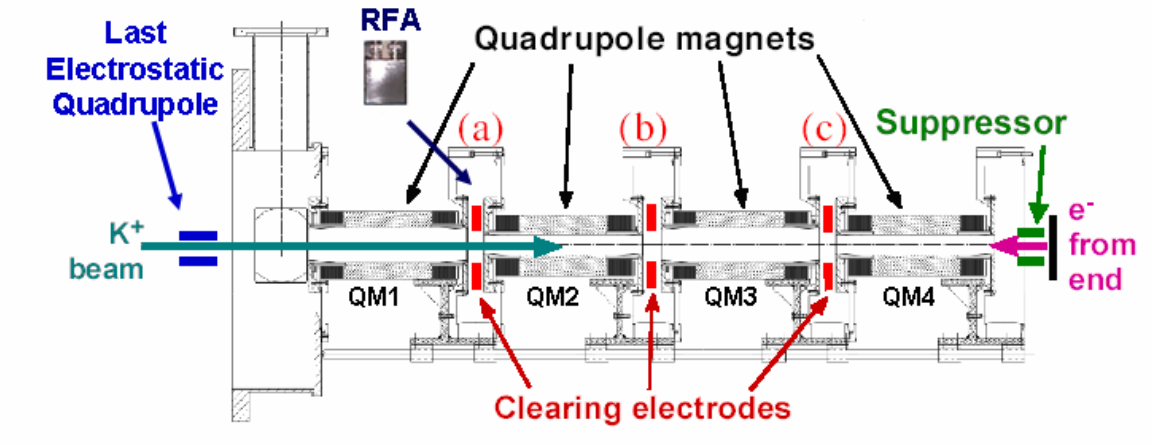

FIG. 1 (color online). Magnetic quadrupole transport section of HCX.

The magnetic section forms an electron trap that can accumulate electrons. Electrons are confined radially by the ~ 2 kV beam space-charge potential and axially by the suppressor at one end and by the last electrostatic quadrupole at the other end, which are biased to -10 kV and -18.6 kV, respectively. Electrons originating from ion impact on structures at the end of HCX can move upstream if the suppressor and clearing electrodes are turned off. Electrons are drained out when they drift to the gaps if the clearing electrodes (A, B and C) are biased to +9 kV.

There are three different sources of electrons that can accumulate within the magnetic section: electrons from ionization of gas, electrons desorbed from beam pipe, and electrons desorbed from the end wall [19].

For the electrons desorbed from the beam pipe, we measured that each 1 MeV K+ ion impacting near grazing incidence on stainless steel desorbs ~ 10,000 molecules of gas and produces ~ 100 electrons [20]. The measured average velocity of the desorbed gas is 1.5 mm/μs [21]; during the beam duration of 5 μs, most of the gas cloud does not expand into the beam path, and consequently it will not be ionized.

Electrons from residual and desorbed gas ionization are produced in an electrostatic potential well formed by the positive beam space-charge; therefore they will be trapped. The total measured beam-background gas interaction cross section (ionization plus charge exchange) is 1.6×10^{-20} m^2 [22], giving an upper limit to the beam neutralization (ratio of electron to the ion charge density) at the end of the pulse of 0.3 %, which is negligible for this experiment.

Ion-induced electrons desorbed from the beam pipe at the beginning of the beam pulse will be trapped by the beam potential that is rising at a rate of ~ 2000 V/μs.

Electron clouds are difficult to measure quantitatively. The trapped electrons are expelled at the end of the beam pulse, when the potential decays. However, in the HCX the beam tail scrapes the wall desorbing new electrons, which confound measurements. In addition simple biased electrodes change the collection length and increase the energy of electron striking the electrodes. Reviews of a variety of diagnostic methods are given in Refs. [1] and [23].

Retarding Field Analyzers (RFA's), which are high-pass energy filters, have been used to measure properties of electron clouds elsewhere [24, 25, 26, 27]. We added an extra repeller grid to Rosenberg's electron analyzer design [28] to allow measuring either ions or electrons. During operation, the clearing electrode A (see Fig. 1) is removed and the RFA, with an energy resolution ($\Delta E/E$) of ~ 0.5 %, is inserted to 4 cm from the axis in

the drift region between quadrupole magnets QM1 and QM2 (gap A), where the magnetic fringe fields vanish.

An illustrative set of RFA collector charge measurements (raw data for the integral of expelled ion current) is given in Fig. 2. The red circles show the time in the RFA signal when the beam potential decays to the potential of the retarding grid (shown in the right side legend), so the ions reflect and cannot reach the collector. With such a series of shots at different retarding potentials, the dynamic beam potential can be determined.

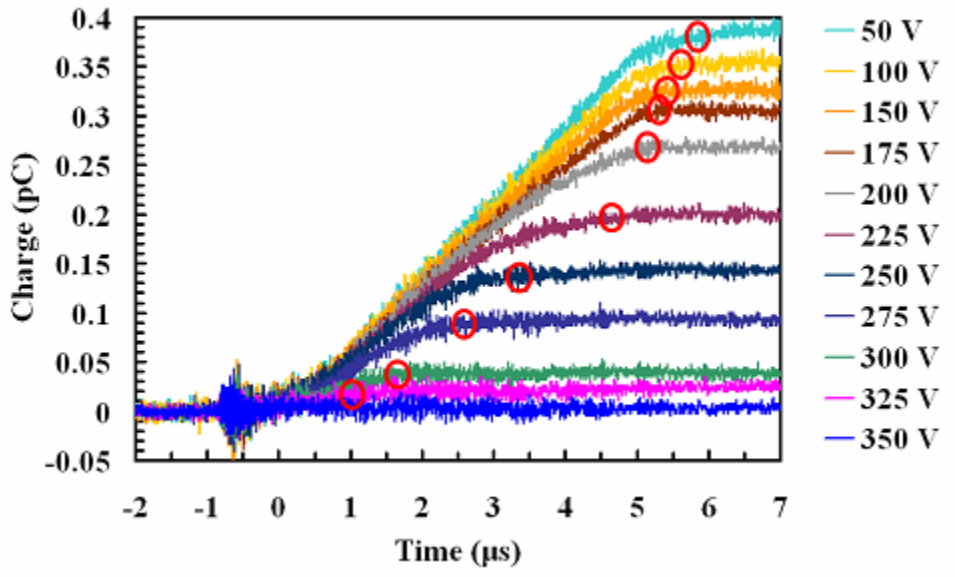

FIG. 2 (color online). RFA collector charge measurements for an apertured beam.

Fig. 3 shows the Faraday cup current (blue line) corrected for the time of flight to the RFA axial location using the left-hand ordinate axis, and the dynamic beam potential using the right-hand ordinate axis for three different conditions. For the first condition the clearing electrodes and the suppressor are all on. The depressed beam potential (red squares) has the same slope as the Faraday cup current, implying that there was no significant beam neutralization during the beam pulse. For the second condition the

clearing electrodes are off and the suppressor is on, which allows electrons from local sources to accumulate, depressing the beam potential by 12% (pink triangles). For the third condition the suppressor and the clearing electrodes are off, which also allows electrons to drift upstream, depressing the beam potential by 43% (green circles).

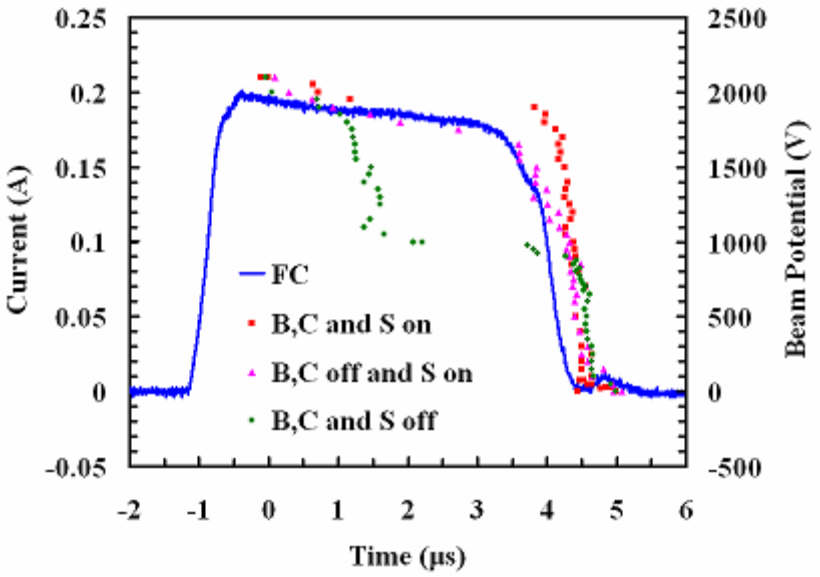

FIG 3 (color online). Dynamic beam potential measured increasing the sources of electrons.

Simulations predict that, when the clearing electrodes and suppressor are off, the electrons ejected from the end wall will drift through quadrupole magnets at a velocity of 0.66 m/μs [29], reaching gap A after 1.44 μs. Measurements from the clearing electrodes show that, when the suppressor and clearing electrodes are off, the electron wave front from the end wall structures propagates at a velocity of 0.60 $\pm$ 0.11 m/μs, in agreement with the simulation.

The electron distribution inside the gaps loses the quadrant structure given by the quadrupole magnetic field [30]. WARP simulations show that the transverse distribution is approximately Gaussian for the electrons and uniform for the ions. The dynamic

electron density is obtained by measuring the fractional reduction of the beam potential with the RFA and multiplying it by 1.68 times the beam density. The factor 1.68 takes into account the broader electron transverse distribution and consequently different space-charge potential contribution.

In Fig. 4, the red and green lines denote the electron currents from clearing electrode A, after subtracting the beam induced capacitive signal, when clearing electrodes B, C and the suppressor are on and off, respectively. The pink line is the sum of the currents from clearing electrodes A, B and C minus the beam induced capacitive signal, when clearing electrodes A, B, C and the suppressor are on. It corresponds to the electron current that should accumulate inside the magnetic section when the clearing electrodes are off and the suppressor is on.

The local electron line charge at gap A for each condition is obtained by dividing the electron current for each configuration shown in Fig. 4 by the average drift velocity, which we designate the "clearing electrode technique". The static background cloud density, which must be added to all the RFA measurements in order to provide absolute measurements, is acquired from the first configuration, when the clearing electrodes B, C and the suppressor are on.

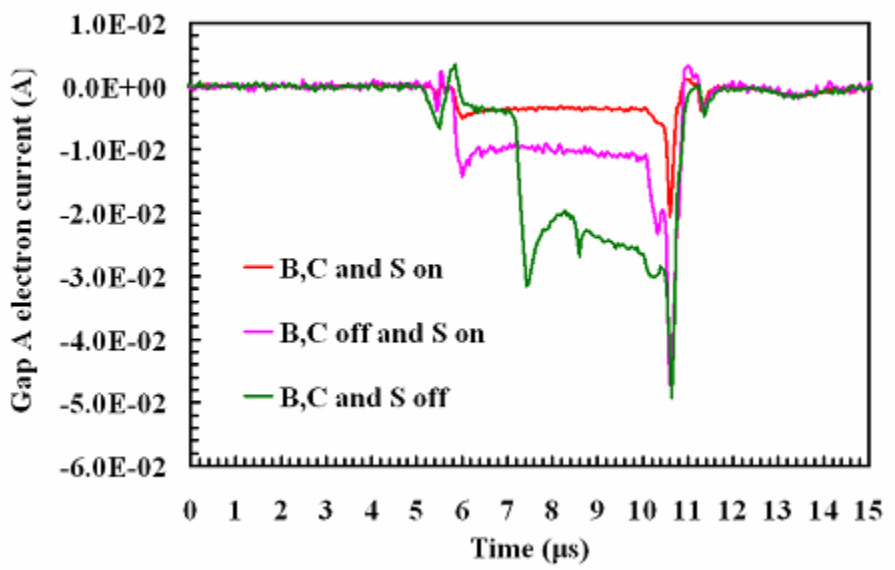

FIG. 4 (color online). Electron current from clearing electrode A obtained for three different configurations.

The average drift velocity ($\overline{v_d}$), needed for the clearing electrode technique, has contributions from $\vec{E}\,x\,\vec{B}$ and $\nabla\vec{B}$ components. The first component is directly proportional to the electric field. The second component is a function of the kinetic energy of the wall-desorbed electrons, which is proportional to the beam potential and consequently to the electric field. Therefore $\overline{v_d}$ is assumed directly proportional to the electric field, which decreases with beam neutralization. As $\overline{v_d}$ ~ 0.60 m/μs for the first configuration (clearing electrodes B,C and suppressor on) is known, we can use the depressed beam potential measured with the RFA to obtain $\overline{v_d}$ for the other configurations.

Beam neutralization	**B, C and S on**	**B, C off and S on**	**B, C and S off**
Clear. Electrodes	**7.3 %**	**25.2 %**	**89.2 %**
RFA	**7.3 %**	**27.5 %**	**79.5 %**

TABLE 1. Comparison of the beam neutralization measured in gap A using the clearing electrode and RFA techniques.

High-current heavy-ion beams are robust to electron clouds. Several percent of the beam neutralization are required for substantial beam degradation of a 200-quadrupole system [19]. The beam neutralization measured in gap A at the end of the beam pulse is summarized in Table 1. Differences between the techniques are probably due to errors in the drift velocity.

Simulations predict 80.7 % beam neutralization in gap C if clearing electrodes B, C and the suppressor are off. When the clearing electrodes are initially on and they are turned off sequentially (C, B and A), the current measured in the last active clearing electrode is the same; consequently the beam neutralization predicted in gap C for the third configuration should be the same as that in gap A and is in excellent agreement with the RFA technique.

An alternative analysis of clearing electrode data is obtained from Fig. 4 if the charge, given by integration of the pink line over the beam duration, is divided by the distance between last electrostatic quadrupole and the suppressor. It gives a beam neutralization of 27.2 % and is in excellent agreement with the Table 1 techniques.

We developed a new technique that measures the time-dependent electron cloud density by probing the depressed beam potential with expelled ions. Sources of electrons are added in three different configurations and the dynamic electron cloud density is measured with the RFA technique. The dynamic density is added to the static density, obtained from the clearing electrode technique, giving an absolute density. Table 1 summarizes the results from both techniques, showing reasonable agreement. We believe that this is the first time-dependent quantitative measurement of electron cloud accumulation during the beam, providing a precise tool to benchmark simulations, and understand the electron cloud physics.

We wish to thank Tak Katayanagi who built the RFA, Wayne G. Greenway, Larry W. Mills and Gary Ritchie who maintain HCX, and Craig Rogers, Ed Romero and William L. Waldron who provided electronic support. We also want to express our gratitude to Richard A. Rosenberg and Katherine C. Harkay for sharing details that aided our RFA design, and to Miguel Furman for his insightful comments. This work was performed under the auspices of U.S. Department of Energy by the University of California, LLNL and LBNL under contracts No. W-7405-ENG-48, and No. DE-AC02-05CH11231.

[1] H. Fukuma, in: Proc. of Diag. Instrum. Part. Acc. Conf., Lyon, France, 2005, p. 122.

[2] G. Budker, G. Dimov, and V. Dudnikov, Sov. Atom. E. **22**, 5 (1967).

[3] O. Gröbner, in: Proc. of 10th Intern. Acc. Conf., Serpukhov, 1977, p. 277.

[4] R. J. Macek et al., in: Proc. of Part. Acc. Conf., Chicago, IL, 2001, p. 688.

[5] S. Y. Zhang et al., in: Proc. of Eur. Part. Acc. Conf., Lucerne, 2004, p. 944.

[6] M. Izawa, Y. Sato, and T. Toyomasu, Phys. Rev. Lett. **74**, 5044 (1995).

[7] K. Ohmi, Phys. Rev. Letters **75**, 1526 (1995).

[8] J. W. Flanagan et al., Phys. Rev. Lett. **94**, 054801 (2005).

[9] W. T. Weng et al., in: Proc. of Part. Acc. Conf., Vancouver, 1999, p. 970.

[10] R. J. Macek, and A. Browman, in: Proc. of Part. Acc. Conf., Knoxville, TN, 2005, p. 2547.

[11] M. A. Furman, LBNL Report No. 50765, 2002.

[12] K. Harkay, and R. A. Rosenberg, Phys. Rev. ST AB **6**, 034402 (2003

[13] R. J. Macek et al., in: Proc. of Part. Acc. Conf., Portland, OR, 2003, p. 3089.

[14] K. Kanazawa et al., in: Proc. of Part. Acc. Conf., Knoxville, TN, 2005, p. 1054.

[15] R. Cimino et al., Phys. Rev. Lett. **93**, 014801 (2004).

[16] J. Klabunde et al., in: Proc. of Part. Acc. Conf., Santa Fe, NM, 1983, p. 2543.

[17] L. R. Prost et al., Phys. Rev. ST AB **8**, 020101 (2005).

[18] J.-L. Vay et al., in: Proc. of Part. Acc. Conf., Knoxville, TN, 2005, p. 525.

[19] R. H. Cohen et al., Phys. Rev. ST AB **7**, 124201 (2004).

[20] A. W. Molvik et al., Phys. Rev. ST AB **7**, 093202 (2004).

[21] F. M. Bieniosek, to be published.

[22] M. Kireeff Covo, to be published.

[23] K. C. Harkay, in: Proc. of ECLOUD, Napa, CA, 2004, http://mafurman.lbl.gov/ECLOUD04_proceedings/harkay_SessionATalk-v2.pdf.

[24] K.C. Harkay, and R.A. Rosenberg, in: Proc. of Part. Acc. Conf., New York, NY, 1999, p. 1641.

[25] T. Toyama, in: Proc. of ECLOUD, Napa, CA, 2004, http://mafurman.lbl.gov/ECLOUD04_proceedings/toyama_ECLOUD04_v4.pdf.

[26] Z. W. Guo et al., in: Proc. of Asian Part. Acc. Conf., Beijing, China, 2001, p. 377.

[27] K. Kanazawa et al., in: Proc. of Part. Acc. Conf., Knoxville, TN, 2005, p. 1054.

[28] R. A. Rosenberg, and K. Harkay, Nucl. Instrum. Methods Phys. Res. A **453**, 507 (2000).

[29] R. H. Cohen et al., LBNL Report No. 56496, 2004.

[30] R. J. Macek, and M. Pivi, http://www-project.slac.stanford.edu/ilc/testfac/ecloud/elecCloud_project3.html